Earth and Planetary Science Letters 528 (2019) 115859

Contents lists available at ScienceDirect

Earth and Planetary Science Letters

www.elsevier.com/locate/epsl

The redox budget of the Mariana subduction zone

Maryjo Brounce [a,*], Elizabeth Cottrell [b], Katherine A. Kelley [c]

[a] Department of Earth Sciences, University of California Riverside, Riverside, CA 92521, USA
[b] Department of Mineral Sciences, National Museum of Natural History, Smithsonian Institution, Washington, DC 20560, USA
[c] Graduate School of Oceanography, University of Rhode Island, Narragansett Bay Campus, Narragansett, RI 02882, USA

ARTICLE INFO

Article history:
Received 12 March 2019
Received in revised form 19 September 2019
Accepted 20 September 2019
Available online 3 October 2019
Editor: T.A. Mather

Keywords:
subduction
Mariana arc
oxygen fugacity
redox
altered oceanic crust
sediment

ABSTRACT

Assessing the efficiency of material recycling at convergent margins is critical to constraining the impact of plate tectonic processes on the composition of surface and deep mantle reservoirs on geologic timescales. In particular, oceanic lithosphere bearing oxidized phases such as Fe-oxy-hydroxides, Fe-oxides, serpentine, carbonate, and sulfate minerals, subduct at convergent margins and the infiltration of aqueous fluids and sediment melts from the subducting slab into the mantle beneath arc volcanoes may thus carry oxidized forms of multi-valent elements (e.g., S, Fe, C) and lead to the generation of primitive arc melts that record elevated oxygen fugacities relative to mid-ocean ridge primitive melts. It is unclear, however, how efficiently aqueous fluids and silicate melts transport the oxidized signatures of any given subducting slab into the mantle wedge in a single subduction zone, and how much, if any, of these oxidized phases may be recycled into the deeper mantle. We present a mass balance of Fe^{3+}, S^{2-}, S^{6+}, and C^{4+}, as well as the O_2 associated with these species, through the Mariana subduction zone to assess the efficiency of recycling oxidized materials in an end-member type subduction zone, where old oceanic lithosphere and a thick sediment package is subducted. To do this, we report $Fe^{3+}/\Sigma Fe$ ratios of bulk sediments and altered oceanic crust recovered from ODP Site 801 in the western Pacific in order to constrain the bulk $Fe^{3+}/\Sigma Fe$ ratio of the Pacific plate prior to subduction in the Mariana convergent margin. Site 801 sediments have $Fe^{3+}/\Sigma Fe$ ratios >0.69 and the altered oceanic crust (801 Super Composite) has $Fe^{3+}/\Sigma Fe$ of 0.51. Bulk $Fe^{3+}/\Sigma Fe$ ratios of altered oceanic crust at Site 801 increase from 0.14 (pristine Jurassic-aged MORB glass) to 0.78 with increasing extent of alteration. We find that 68–95% of the O_2 added to the subducting crust by sedimentation, *in situ* alteration of basaltic crust on the seafloor, and serpentinization of the mantle lithosphere is not output by Mariana arc or back-arc magmas. This result demonstrates that significant amounts of oxidized materials from Earth's surface are transported into the deeper mantle beyond subduction zones, despite the production of oxidized arc and back-arc basalts, and may contribute to elevated oxygen fugacities recorded by ocean island lavas such as Iceland and Hawaii. This oxygen cycle is likely to have been operating at least for the past 400–800 million years, and potentially for the duration of plate tectonics.

1. Introduction

Surface materials are physically mixed into the mantle at convergent margins, and the extent to which these materials are returned to the surface in subduction zone volcanism is critical to understanding the impact of subduction on the composition of Earth's mantle on geological timescales. The subduction of oxidized materials and the potential link to the oxidized nature of subduction zone volcanism has been recently debated. Sediments containing organic (reduced) and inorganic (oxidized) carbon are deposited on the seafloor as it ages. Ferric-iron bearing phases such as celadonite and Fe-oxyhydroxides and ferrous-iron bearing phases such as saponite and pyrite precipitate within the basaltic crust due to interactions between silicate rocks and oxic seawater (Alt and Teagle, 2003; Lecuyer and Ricard, 1999; Rouxel et al., 2003). Ferrous iron-bearing phases such as olivine and pyroxene are replaced with ferric iron-bearing phases such as magnetite and serpentine-group minerals during serpentinization of ultramafic rocks (Andreani et al., 2013; Marcaillou et al., 2011; Klein et al., 2009). Eventually, these lithological signatures of the oxic and wet conditions at Earth's surface subduct at convergent margins. There is general agreement that aqueous fluids and silicate melts emanating from subducting slabs play a fundamental role in setting the trace element and isotopic compositions of

* Corresponding author.
E-mail address: maryjo.brounce@ucr.edu (M. Brounce).

https://doi.org/10.1016/j.epsl.2019.115859
0012-821X/

arc lavas globally (e.g., Morris and Tera, 1989; Plank and Langmuir, 1998; Elliott et al., 1997). Additionally, arc basalts have a higher proportion of Fe^{3+} relative to mid-ocean ridge basalts, and this may be linked to the potential of the oxidized phases contained within subducting slabs to influence the availability of oxygen in aqueous fluids and silicate melts derived from them during subduction (e.g., Brounce et al., 2014; Evans, 2012; Kelley and Cottrell, 2009; Mungall, 2002; Parkinson and Arculus, 1999; Wood et al., 1990). However, the mechanisms and efficiency of the transfer of oxygen from specific phases contained in seafloor sediments, altered oceanic crust, and mantle lithosphere to primary arc magmas are difficult to assess directly due to the nature of material mixing at the slab surface-mantle wedge interface. Estimates of the fluxes of Fe^{3+}, S^{6+} and C^{4+} have been calculated from globally averaged plate rates and compositions, finding that subduction zone recycling of oxidized materials back to the surface in arc volcanism is generally inefficient, and leads to a net influx of oxidized materials into the deep mantle on geological time scales (Lecuyer and Ricard, 1999; Hayes and Waldbauer, 2006; Evans, 2012). The inefficiency of recycling oxidized materials at subduction zones has also enabled recent hypotheses that oxidized, altered oceanic crust in the Hawaiian, Icelandic, and Erebus mantle plumes contribute to the production of lavas with elevated $Fe^{3+}/\Sigma Fe$ ratios relative to mid-ocean ridge basalts (MORB; Moussallam et al., 2014; Moussallam et al., 2016; Brounce et al., 2017; Helz et al., 2017; Shorttle et al., 2015).

The expected magnitude of the deep subduction of surface-derived oxygen may be subtle on the basis of mass balance arguments (e.g., Sleep et al., 2012), or a significant mechanism for buffering surface pO_2 on 10 s of million of years timescales (e.g., Lecuyer and Ricard, 1999; Evans, 2012; Duncan et al., 2017). However, globally averaged constraints such as those presented by Lecuyer and Ricard (1999) and Evans (2012) potentially obfuscate the relationships between atmospheric pO_2 and solid Earth fO_2. For example, subduction zones that are active today vary widely in the composition and flux of sediments being recycled, the age and extent of alteration of oceanic crust being subducted, the extent of serpentinization of the underlying lithosphere, the extent to which sediments and oceanic crust are returned to the arc crust during subduction, and the composition and flux of material erupted at arc volcanoes. A globally averaged balance of the inputs and outputs of O_2, Fe^{3+}, C^{4+}, and/or S^{6+} to the Earth's mantle thus has large uncertainties. Establishing quantitative links between direct measurements of the altered, subducting crust, mantle lithosphere, and sediments and the magmas emplaced in the arc and back-arc crust in a single, end-member convergent margin system, however, provides a unique constraint on the efficiency of elemental transfer within a modern subduction zone. In addition, recent constraints on the effects of low pressure differentiation on the $Fe^{3+}/\Sigma Fe$ ratios of erupted arc and back-arc basalts (Brounce et al., 2014; Kelley and Cottrell, 2012) present the opportunity to incorporate firm constraints on the oxidation state of Fe in primitive subduction related basalts into mass balance calculations of this kind for the first time at a specific arc.

Here, we present measurements of the $Fe^{2+}O$ abundance in lithologies representative of inputs to the Mariana convergent margin, determined by whole-rock wet chemistry, in order to constrain the bulk oxidation state of material entering the subduction zone. We pair these new data with previously collected major element concentrations on the same samples (Fisk and Kelley, 2002; Kelley et al., 2003) to calculate $Fe^{3+}/\Sigma Fe$ ratios (i.e., $Fe^{3+}/[Fe^{2+} + Fe^{3+}]$), as well as with previously reported measurements of organic carbon to carbonate (Lancelot et al., 1990; Sadofsky and Bebout, 2004), and sulfide to sulfate (Rouxel et al., 2008) on samples from the same locations. These data constrain the proportion of oxidized Fe, S, and C in the subducting sediment and the extent to which their net oxidation states have changed during sedimentation and alteration of oceanic crust. We demonstrate that post-eruptive alteration elevates $Fe^{3+}/\Sigma Fe$ ratios in basaltic oceanic crust and that this alteration persists uniformly to 500 m depth into igneous basement, consistent with previous work in obducted ophiolite terranes (e.g., Gillis and Robinson, 1990). In the absence of recovered materials from the mantle lithosphere portion of the Pacific plate, we combine our measurements from ODP 801 materials with the average abundance of oxidized Fe, S, and C in serpentinized peridotites from Evans (2012) and estimates of the extent of serpentinization of the Pacific plate from Cai et al. (2018). We use the values of Evans (2012) and those calculated here to calculate a mass balance for Fe^{3+}, S^{6+}, and C^{4+}, and the equivalent O_2 bound to these cations (i.e., the O_2 necessary to form Fe_2O_3, SO_4^{2-}, and CO_3^{2-}) through the Mariana subduction system (Fig. 1), in order to determine the efficiency with which the oxidized state of a subducting slab passes through the subduction filter.

2. Methods

2.1. ODP Site 801 materials and sample selection for this study

Ocean Drilling Program Site 801 sits east of the Mariana subduction zone in Pacific plate that will eventually be consumed by subduction at the Mariana trench. As such, it represents the crustal inputs to the Mariana subduction zone and has been established as a geochemical reference site for the Mariana arc (Kelley et al., 2003; Plank et al., 2000). Drilling during ODP Legs 129 and 185 recovered 465 m of sediment and the upper 470 m of 170 my old altered, basaltic oceanic crust (Lancelot et al., 1990; Plank et al., 2000; Fig. 1). Kelley et al. (2003) and Plank et al. (2000) report major and trace element geochemistry of powdered samples of sediment, altered oceanic crust, and mixed composite powders recovered from ODP Site 801.

The basal sediments recovered from ODP Site 801 are composed of radiolarite and siliceous claystones, overlain by brown radiolarite and manganiferous dark brown chert. These sedimentary units are overlain by pervasively altered volcaniclastic turbidites that contain secondary mineralization composed of smectites, celadonite, clinoptilolite, phillipsite, analcime, calcite, and quartz. This is overlain by brown chert and porcellanite, and the section is capped with zeolitic pelagic brown clay (Karpoff, 1992; Fig. 1). Basalts recovered at ODP Site 801 are 10–20% recrystallized via alteration; alteration products consist saponite, calcite, celadonite, iron oxyhydroxides, and pyrite (Alt and Teagle, 2003).

We selected powders of each major sedimentary and altered oceanic crust lithology from Site 801. Though the number of samples analyzed in this study is small relative to the heterogeneity of core materials, we believe that these samples represent each major unit that is well-defined geochemically and lithologically (e.g., Plank and Langmuir, 1998). For each selected sample, splits were taken from the exact powder samples that had previously been measured for major and trace element chemistry (Kelley et al., 2003; Plank et al., 2000). We present measurements of 9 sediment samples (pelagic clays, chert, porcellanite, radiolarite, volcanic turbidite), 8 variably altered MORBs (from fresh pillow glass to pervasively altered), 1 hydrothermal deposit, 2 iron oxide veins, 2 hyaloclastites, and 8 mixed composite powders from the sediment and upper 500 m of altered oceanic crust. The composite powders are physical mixtures of discrete materials from the recovered core (Kelley et al., 2003). Individual samples were mixed in proportions equal to their abundance in recovered cores and thus serve as single reference powders for portions of the Site 801 core. These composite powders were designed to characterize large

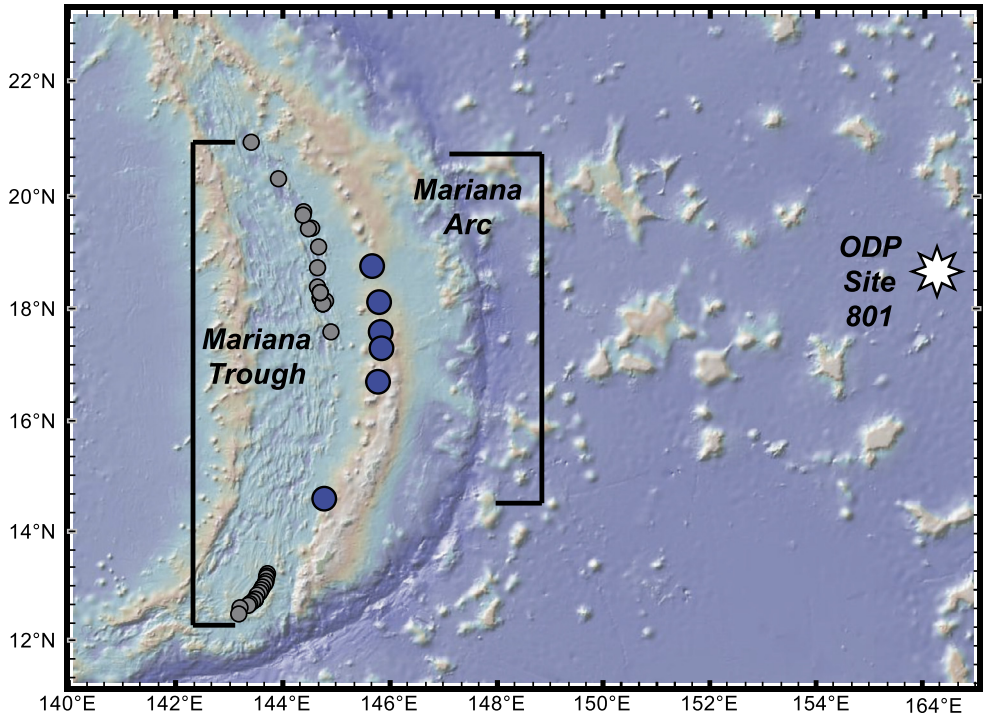

Fig. 1. Location map for samples used in this study. Blue circles mark the position of Mariana arc volcanoes, from which the $Fe^{3+}/\Sigma Fe$ ratios of both melt inclusions and submarine glasses were used to constrain the flux of Fe^{3+} out of the volcanic arc (Brounce et al., 2014). The dark gray circles mark the position of submarine glass samples that were used to constrain the flux of Fe^{3+} out of the back-arc (Brounce et al., 2014). The position of ODP Site 801 is marked with the white star. The basemap was created using GeoMapApp (Ryan et al., 2009). (For interpretation of the colors in the figures, the reader is referred to the web version of this article.)

sections of the basement crust, maximizing the number of analyses that could be performed on a single representative sample. We take advantage of that approach here by layering on new measurements of $Fe^{2+}O$.

2.2. Analytical methods for microcolorimetry

We determined $Fe^{2+}O$ concentrations in selected rock and sediment powders following the micro-colorimetric methods described by Wilson (1960) and Carmichael (2014). Analyses of these USGS standards never deviated from the certified $Fe^{2+}O$ content by more than 0.46 wt% (absolute) for the lowest $Fe^{2+}O$ standard (QLO-1, 2.97 wt%) and by 0.27 wt% (absolute) for the highest $Fe^{2+}O$ standard (BCR-1, 8.8 wt%; Table 2). The detection limit for this procedure is conservatively estimated to be 0.25 wt% $Fe^{2+}O$.

3. Results

Analytical results are presented in Tables 1 and 2. Pristine glass chips with no sign of devitrification or alteration from ODP Site 801, measured by XANES (Brounce et al., 2015), have the same $Fe^{3+}/\Sigma Fe$ ratios as modern MORB glass (~0.14; Cottrell and Kelley, 2011; Zhang et al., 2018), indicating that before alteration, the igneous basement had a similar bulk redox state to modern MORB and that the upper mantle source of Pacific Ocean spreading centers has not varied significantly from the Jurassic to present day. Whole-rock basalts described as "minimally altered" by the science party at the time of drilling (Kelley et al., 2003) are more oxidized (0.29–0.46 $Fe^{3+}/\Sigma Fe$; Fig. 2), which demonstrates that even minor alteration can oxidize Fe in basaltic rocks. The oxidation state of Fe increases with increasing extent of alteration (0.47–0.78 $Fe^{3+}/\Sigma Fe$ in samples described as pervasively altered; Kelley et al., 2003) and the samples that include iron oxide veins, alteration halos, and celadonite contain mostly Fe^{3+} (0.69–0.95 $Fe^{3+}/\Sigma Fe$; Fig. 2). The overlying sediments are oxidized (0.69–0.95 $Fe^{3+}/\Sigma Fe$). Some of these sediment samples have low FeO^* (i.e., total Fe expressed as FeO) that when combined with their bulk oxidation state, reflect low $Fe^{2+}O$ concentrations which likely approach the detection limit of the wet chemical methods used here (0.25 wt% $Fe^{2+}O$; Table 1, Fig. 2). The range in $Fe^{3+}/\Sigma Fe$ ratios span the value expected from melting of the upper mantle (~0.14) to almost entirely comprising Fe^{3+} (~0.95), demonstrating that although the total number of samples measured is small, we have captured the full range of possible values. Two black arrows on Fig. 2 show the $Fe^{3+}/\Sigma Fe$ ratios of composite powders. The 801 Super Composite, intended to represent the bulk composition of the upper 500 m of altered oceanic crust at Site 801, has an $Fe^{3+}/\Sigma Fe$ ratio of 0.51. We note that the oxygen isotope compositions reveal that the 801 Super Composite powder contains a higher proportion of interflow sediment materials than may be present in the cored materials (Alt and Teagle, 2003), but the broad consistency between the average $Fe^{3+}/\Sigma Fe$ ratios of discrete samples and that of 801 Super Composite powder indicates that this does not impact $Fe^{3+}/\Sigma Fe$ significantly. The 801 SED composite, made up of representative interflow material within the altered oceanic crust at Site 801, has a lower $Fe^{3+}/\Sigma Fe$ ratio than the range observed for true sediment materials in the overlying sediment package (0.67, Fig. 2). The other MORB composite powders, mixed to represent specific depth intervals, have a small range from 0.51–0.52 $Fe^{3+}/\Sigma Fe$ (Table 1). This constancy demonstrates that, at a minimum, the upper 500 m of igneous basement at ODP Site 801 has been affected by alteration reactions that increase the $Fe^{3+}/\Sigma Fe$ ratios of bulk oceanic crust over the original igneous value. Two composite powders from a massive alkali basalt flow (Top Alkali Basalt, TAB-FLO; Kelley et al., 2003) and the highly altered interflow material associated with that flow (TAB-VCL; Kelley et al., 2003) have $Fe^{3+}/\Sigma Fe$ ratios of 0.40 and 0.38, respectively. These units are younger than the MORB tholeiites (157 Ma for TAB vs. 165–170 Ma for MORB; Fisk and Kelley, 2002) and not thought to be representative of normal MORB oceanic crust. As a result, they may

Table 1
Fe redox analyses for ODP Site 801 discrete samples and composite powders.

Sample	Meters below seafloor	Unit description	$Fe^{2+}O$ (wt%)	FeO* (wt%)[a]	$Fe^{3+}/\Sigma Fe$	$Fe^{3+}/\Sigma Fe$ (Rouxel et al., 2003)
Discrete 801 powders						
801A3R2-145	15	pelagic clay	below detection	6.60		>0.99
801A5R3-145	36	pelagic clay	below detection	5.43		>0.99
801A8R1-1	60.6	chert	below detection	0.27		
801A17R1-28	147.5	porcellanite	0.99	3.24	0.69	
801A19R1-65	167	volcanic turbidite	1.13	5.78	0.80	
801B5R2-0	225	volcanic turbidite	2.19	8.91	0.75	
801B25R1-49	397.7	radiolarite	0.18	1.98	0.91	
801B33R1-143	436	radiolarite	0.64	6.54	0.90	
801B35R3-19	455.5	radiolarite + claystone	0.34	8.82	0.96	
801B37R1-36	461.9	uppermost basalt, pervasively altered	0.76	3.52	0.78	
801B41R1-26	483.3	minimally altered basalt	6.10	9.59	0.36	
801B43R1-132	493.5	minimally altered basalt	6.13	11.25	0.45	
801B43R3-111	496.1	minimally altered basalt	3.90	7.21	0.46	
801C4R1-72	522.4	hydrothermal deposit	0.53	11.50	0.95	>0.99
801C5R1-95a	532.2	pervasively altered basalt with celadonite	0.97	5.35	0.82	0.88
801C15R7-31	621.7	bleached basalt	2.44	5.05	0.52	0.67
801C19R2-24a	653.4	hyaloclastite	2.16	11.33	0.81	
801C24R1-46	691.8	pervasively altered basalt	7.20	13.59	0.47	
801C30R1-111a	748.4	minimally altered basalt	9.21	13.83	0.33	
801C31R4-43	761.0	minimally altered basalt	9.72	13.67	0.29	
801C34R1-93a	786.2	iron oxide vein, alteration halo	6.81	14.11	0.52	
801C38R3-53a	826.3	hyaloclastite and pillow margin	4.74	15.42	0.69	
801C52MI47a	933.3	minimally altered basalt	7.44	12.29	0.39	
Composites (Kelley et al., 2003)						
801SED		interflow sediments in igneous basement	2.91	8.75	0.67	
801SUPER		bulk composition of altered igneous crust	6.01	12.34	0.51	
801TAB-VCL		alkali basalt volcaniclastic sediments	3.97	6.43	0.38	
801TAB-FL0		alkali basalt flow	5.36	8.95	0.40	
801TAB0-50		bulk composition of top 50 m of alkali basalt	4.92	8.35	0.41	
801M0RB0-110		bulk composition of top 110 m of MORB	5.56	11.45	0.51	
801M0RB110-220		bulk composition of MORB 110–220 m	6.02	12.35	0.51	
801M0RB220-440		bulk composition of MORB 220–440 m	6.24	13.10	0.52	

[a] Total Fe expressed as FeO*, from Kelley et al. (2003).

Table 2
$Fe^{2+}O_{(actual)}$ for USGS standard powders.

Standard	$Fe^{2+}O_{(actual)}$ (wt%, measured)	$Fe^{2+}O_{(actual)}$ (wt%, published)
QLO-1	3.26	2.97
1σ	0.18	
n	6	
BCR-1	8.87	8.80
1σ	0.20	
n	5	
BIR-1	8.72	8.34
1σ	0.10	
n	7	

have had a different starting $Fe^{3+}/\Sigma Fe$ ratio than MORB tholeiites and potentially different alteration histories (Kelley et al., 2003; Plank et al., 2000).

4. Discussion

In order to assess the efficiency of recycling of oxidized components in the Mariana subduction system, we first calculate the average concentrations of Fe^{3+}, S^{6+}, S^{2-}, and C^{4+} present in ODP Site 801 sediments and altered oceanic crust, as well as in pristine mid-ocean ridge, arc and back-arc basalts, using data presented in this study, recent Fe-XANES studies (e.g., Brounce et al., 2014; Brounce et al., 2015; Cottrell and Kelley, 2011; Zhang et al., 2018), and other publications measuring the same or similar materials (Lancelot et al., 1990; Karpoff, 1992; Rouxel et al., 2008). With these average concentrations, and those reported by Evans (2012) for serpentinized peridotite, we calculate the mass fluxes of each species into and out of the mantle as the result of sedimentation and alteration of the seafloor at Earth's surface, as well as due to mid-ocean ridge, arc and back-arc volcanism. For each mass flux, we calculate the oxygen equivalent mass flux as O_2 to balance S^{6+} as SO_4^{2-}, C^{4+} as CO_3^{2-}, and Fe^{3+} as Fe_2O_3 on the basis of stoichiometry. Finally, through comparison of the calculated oxygen fluxes in each setting (i.e., mid-ocean ridge, arc, and back-arc volcanism; subduction of altered crust, seafloor sediments, and mantle lithosphere) we constrain the flux of oxygen into the Pacific plate during sedimentation and alteration on the seafloor, and the flux of that surface-derived oxygen into the deep mantle after shallow recycling at the Mariana subduction zone.

4.1. Oxidized sediments and oxidation of basaltic crust

The iron in the pelagic/biogenic sediments is predominantly present as ferric iron (Table 1). These units are also dominated by carbonate, with the exception of the topmost pelagic clay section, which has abnormally high organic carbon concentrations that is not representative of the organic carbon contents of seafloor sediments in the western equatorial Pacific (Lancelot et al., 1990). This high organic carbon measurement will not be considered in the calculations described below. Instead, we use organic carbon contents reported for Site 801 and nearby Site 800 (Sadofsky and Bebout, 2004; Table 3). The pelagic sediments are also dominated by sulfate (Alt and Burdett, 1992; Table 3). In the volcanic turbidite sections, it is clear that the alteration reactions that lead to the precipitation of ferric iron-bearing smectite minerals and celadonite dominate the effect of alteration on the bulk oxidation state of iron in the sample, evidenced by the elevated $Fe^{3+}/\Sigma Fe$ ratio of the samples studied here (Table 1, Fig. 2). Car-

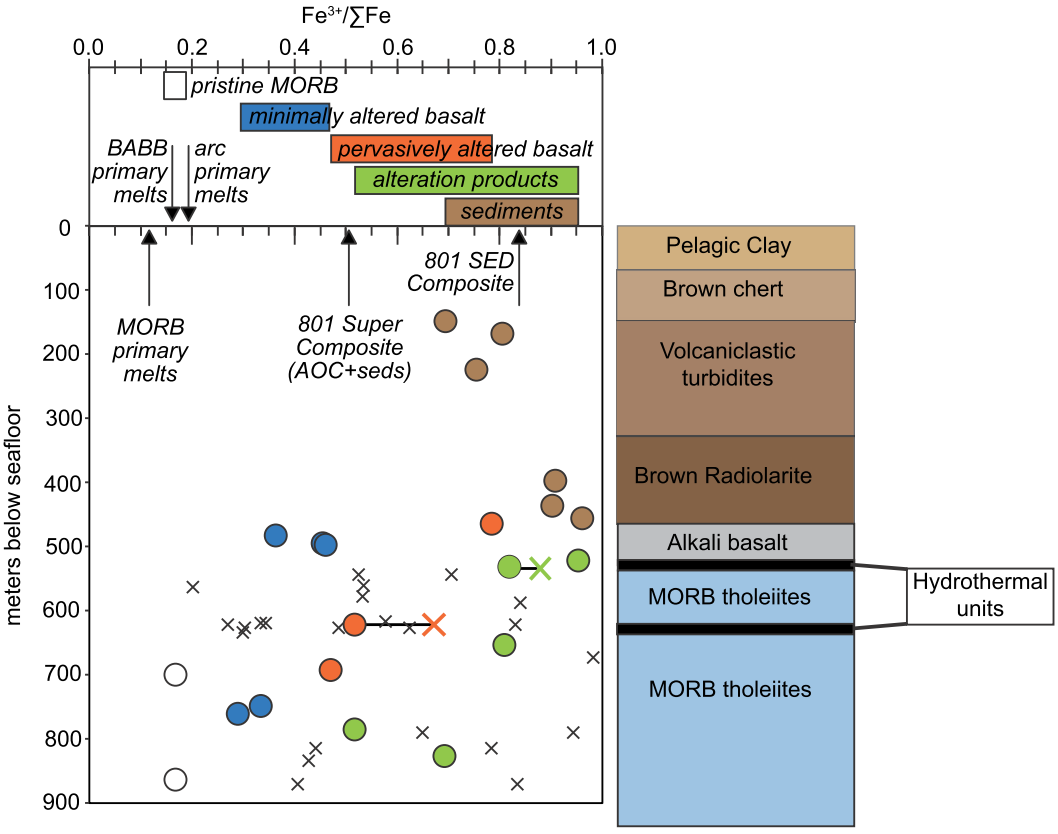

Fig. 2. The $Fe^{3+}/\Sigma Fe$ ratios of materials in this study (brown, green, orange, and blue circles). Top panel: boxes show the range in $Fe^{3+}/\Sigma Fe$ ratios observed for materials of each type. Arrows point to constraints for the 801 Super Composite and average sediments (this study), average primary mantle melts for back-arc basin (Brounce et al., 2014), arc basalts (Brounce et al., 2014), and MORB (Zhang et al., 2018). Bottom panel: The $Fe^{3+}/\Sigma Fe$ ratios from measurements of discrete samples versus their position in the drill core. Colored circles correspond to the labels in the top panel (white = pristine MORB; blue = minimally altered basalts; orange = pervasively altered basalt; green = alteration products; brown = sediments). The *x* symbols represent the $Fe^{3+}/\Sigma Fe$ ratios determined on materials from the same core by Rouxel et al. (2003), for comparison. Two samples that measured here and by Rouxel et al. (2003) are connected via a black tie-line. The white circles show the $Fe^{3+}/\Sigma Fe$ ratios of two pristine MORB glass chips, determined via Fe-XANES (Brounce et al., 2015).

bonate dominates over organic carbon in the remainder of the sediments (Lancelot et al., 1990), and though sulfide proportions increase slightly in the volcanic turbidite and radiolarite sections, these sediments remain dominated by sulfate. The total sulfur concentrations of any sediment unit recovered from Site 801 remain well below 1 wt%, and typically fall between 20–2000 ppm total sulfur (Alt and Burdett, 1992; Table 3). In the basaltic section of ODP Site 801, ferric iron-bearing celadonite and iron oxyhydroxide are precipitated in alteration halos as the result of seawater circulation through fractures in the oceanic crust (Alt and Teagle, 2003). Ferrous iron-bearing saponite and pyrite are also precipitated along fractures in zones of restricted seawater circulation, but results from this study indicate that the net result of alteration on the seafloor is to oxidize Fe and increase the $Fe^{3+}/\Sigma Fe$ ratio of the seafloor sediments and oceanic crust portions of the seafloor (Fig. 2). Altered basalts also have >1000 ppm carbonate, which is elevated over the ~100–300 ppm CO_2 of partially degassed mid-ocean ridge magmas (Saal et al., 2002; Le Voyer et al., 2017; Table 3). Sulfur contents of the altered portions of the oceanic crust are both elevated and depleted relative to fresh basalt such that the average, or "bulk" altered oceanic crust at Site 801 has similar total sulfur contents as fresh basalt (Rouxel et al., 2008; Table 3).

4.2. Mass balance

In order to assess the fate of these oxidized components, we present a mass balance calculation for Fe^{3+}, C^{4+}, and S^{6+} through the Mariana subduction system, using data presented here and in previously published work (Brounce et al., 2014, recalibrated according to Zhang et al., 2018; see supplement). Implicit in such a calculation is the assumption that Fe^{3+}, C^{4+}, and S^{6+} are conserved elements, i.e., there is a fixed concentration of each element that is redistributed during subduction and its valence state does not change. This is likely not the case. Iron can change oxidation state amongst Fe^0, Fe^{2+}, and Fe^{3+} in solid Earth materials depending upon the composition (including the oxygen fugacity) of the system. Similarly, carbon can exist as C^{4-} (i.e., organic carbon) to C^{4+} (i.e., carbonate), and sulfur occurs predominantly as S^{2-} or S^{6+}. Materials in subducting slabs, the melts and fluids that come off of the slab during subduction, the mantle wedge, melts of the mantle wedge, and the upper mantle under ocean islands all may exist in a range of fO_2 where Fe^{2+}, Fe^{3+}, S^{2-}, S^{6+}, C^{4-}, and C^{4+} coexist and electronic exchange can take place between the elements in order to satisfy the fO_2, P, T, and compositional constraints on the system. Though Fe^{3+}, C^{4+}, and S^{6+} are useful tracers for oxygen uptake in altered oceanic crust, one or more of these species in fixed quantities are not necessarily mobilized from the slab to the wedge when the fluids or melts are released from the slab. In other words, the portions of the mantle wedge that are impacted by recycling materials from the subducting slab are an open system to oxygen. It is not clear at this time which specific phases are mobilized during subduction that translate this oxygen potential (e.g., it could be aqueous S^{6+}; Kelley and Cottrell, 2009; Gaillard et al., 2015, or Fe^{3+}; Mungall, 2002; or even S^{2-}; D'Souza and Canil, 2018). For this reason, we calculate the O_2 necessary to balance Fe^{3+} as Fe_2O_3, C^{4+} as carbonate, and S^{6+} as sulfate. We include this O_2 calculation as part of the mass balance calculations

below. Specific values used in these calculations, as well as the results of these calculations, are displayed in Table 4.

4.2.1. Abundance of ferric iron, carbonate and organic carbon, and sulfide and sulfate in Pacific oceanic crust, mantle, and seafloor sediments

To calculate the Fe^{3+} content of material entering the mantle at the Mariana subduction zone, we take the lithologically weighted average $Fe^{3+}/\Sigma Fe$ ratios and FeO* concentrations of discrete sediment samples from Site 801 (see supplement) and altered crust of the 801 Super Composite to represent the $Fe^{3+}/\Sigma Fe$ ratios of bulk sediment and the upper 470 m of bulk altered oceanic crust, respectively, in the Pacific plate prior to subduction. We use an average measured sediment porosity of 24% (after Kelley et al., 2005). We assume that the ~6.5 km of underlying dike and gabbro units are unaltered (Alt et al., 1986), that the dike units have $Fe^{3+}/\Sigma Fe$ ratio and FeO* equal to that of pristine MORB glass from ODP Site 801, and that the gabbro and dike units should have $Fe^{3+}/\Sigma Fe$ ratio and FeO* that sum to that of a primary melt of the ODP Site 801 glass that represents the dike units. We calculate this primary melt composition by adding olivine back to the composition of sample 801C-28R2-118 (Brounce et al., 2015) until it is in equilibrium with Fo_{90} olivine using an FeO/MgO K_D of 0.3. These constraints yield a calculated $Fe^{3+}/\Sigma Fe$ ratio for the whole crust of 0.143 (altered crust + dikes + gabbros), which is slightly below estimates from Lecuyer and Ricard (1999; 0.16–0.20). We use $Fe^{3+}/\Sigma Fe$ ratios and FeO* from Evans (2012) for serpentinized mantle lithosphere. From seismic observations of the Pacific plate near the Mariana trench, we assume that serpentinization extends to at least 24 km depth from the Moho within the plate (Cai et al., 2018). The degree of serpentinization over this interval is uncertain; we use a conservative estimate for the entire interval of 10%.

The total input flux of Fe^{3+} to the Mariana trench from the subducting sediments, altered oceanic crust, and mantle lithosphere can then be calculated following the methods outlined by Kelley et al. (2005) and Lecuyer and Ricard (1999), using the equation:

$$F_{in} = \sum z_i * \rho_i * v_i * [Fe^{3+}]_i \quad (1)$$

where z_i is the thickness of layer i, ρ_i is the density of layer i, v_i is the convergence rate (5.475 cm/yr; Kato et al., 1998), and $[Fe^{3+}]_i$ is the concentration of Fe^{3+} calculated from $Fe^{3+}/\Sigma Fe$ ratios determined here for layer i (see Table 4). Summing over each layer yields a total input flux for Fe^{3+} of 274 kg/yr/cm arc length, or 118 kg/yr/cm arc length equivalent O_2 (Table 4). A significant portion of this comes as the result of oxidation on the seafloor, so we also calculate the Fe^{3+} content of pristine MORB to estimate how much of this input flux was generated at the mid-ocean ridge and how much is the result of alteration. We use the same constraints for the dike and gabbro units as above, except that we treat the altered igneous basement layer from ODP Site 801 as an unaltered basalt unit with $Fe^{3+}/\Sigma Fe = 0.151$ (Brounce et al., 2015), and assume that prior to being infiltrated with or exposed to seawater, the mantle lithosphere is not serpentinized.

Assuming a crustal production rate at mid-ocean ridges equal to the rate of subduction, we estimate that pristine MORB has an output flux of 129 Fe^{3+} or 55 O_2 (kg/yr/cm arc length, Fig. 3). The difference in the fluxes for altered Pacific plate and pristine MORB (145 Fe^{3+}, or 62 O_2 kg/yr/cm arc length) represents the total amount of Fe^{3+} produced as the result of alteration on the seafloor and the deposition of seafloor sediments on top of the oceanic crust between the time the lithosphere formed and the time that the slab will be subducted (Table 4). About 9% of the value of this flux derives from the sediment column, 17% is contributed from the 470 m of altered basaltic crust, and the remaining 74% from the serpentinized mantle lithosphere.

Table 3
Calculated carbon and sulfur contents of ODP 801 materials.

	Thickness (m)	S^{6+} (ppm)[a]	S^{2-} (ppm)[a]
Pelagic clay	60.6	1795	5
Porcellanite and chert	106.4	0	0
Volcaniclastic sediments	230.7	313	83
Radiolarite	64.2	490	10
	weighted average[e]	***460***	***37***
	Thickness (m)	S^{6+} (ppm)[b]	S^{2-} (ppm)[b]
Altered oceanic crust	471.3	1047	1003
801 Super Composite		257	662
	Thickness (m)	C^{4+} (wt%)[c]	C^{4-} (wt%)[c]
Pelagic clay	60.6	1.80	0.06
Porcellanite and chert	106.4	0.14	0
Volcaniclastic sediments	230.7	0.45	0
Radiolarite	64.2	0.02	0
		0.99	0.01
	Thickness (m)	C^{4+} (wt%)[d]	C^{4-} (wt%)[d]
Altered oceanic crust	471.3	0.63	0.00

*For the majority of studies referenced in footnotes a–d, those studies have no measured the same samples from this study. However, all studies report measurements of the main lithologies present in each section of Site 801 core and we take those measurements as representative of the lithologies studied here, and conclude that they are comparable.

[a] Data from Alt and Burdett (1992), Table 2.
[b] Data from Rouxel et al. (2008), Table 1.
[c] Data from Lancelot et al. (1990), Table 3, p. 111 and Sadofsky and Bebout (2004).
[d] Data from Floyd and Castillo in Lancelot et al. (1990), Tables 3 and 4.
[e] Weighted averages are calculated by multiplying the average concentrations of indicated species reported for the indicated layers reported by the studies indicated in footnotes a–d by the thickness of each layer.

Previous global estimates attribute a higher proportion of the total surface oxidation to altered oceanic crust (93%; Lecuyer and Ricard, 1999). The most important difference between that study and this and the work of Evans (2012) is that Lecuyer and Ricard (1999) did not consider serpentinized mantle lithosphere. Other, smaller differences reflect the range in possible subduction configurations: the Marianas represents an end-member style of subduction in that there is a thick sediment package that is fully subducted. Evans (2012) attributed a lower proportion of the total surface oxidation to serpentinized mantle lithosphere. This highlights (a) the magnitude of the uncertainty in the extent of serpentinization in downgoing slabs, and (b) the extent of variability that can be expected in terms of the input flux of surface derived materials to the mantle at subduction zones.

The same calculations can be done for carbonate, organic carbon, sulfide, and sulfate contained in the sediments and crust. To calculate the concentrations of each species in the sediment column entering the mantle at the Mariana subduction zone, we take the average concentrations of each species from discrete sediment samples in the same way as for Fe, using data from other studies (organic carbon, carbonate from Lancelot et al., 1990; Sadofsky and Bebout, 2004; sulfate and sulfide from Alt and Burdett, 1992). For the sediment column, this approach yields weighted averages of 0.99 wt% carbonate, 0.25 wt% organic carbon, 37 ppm sulfide, 460 ppm sulfate (Table 3). For sulfur, we use measurements of the 801 Super Composite powder (Rouxel et al., 2008; Table 3) to represent the upper 470 m of bulk altered oceanic crust (note that this value of sulfate is likely to be a maximum estimate due to post-recovery oxidation; reassigning the sulfate to sulfide has a negligible effect on the calculations presented here). For carbon, in the absence of measurements of

Table 4
Mass balance Fe^{3+} calculation.

	$Fe^{3+}/\Sigma Fe$[a]	FeO* (wt%)	Fe^{3+} (wt%)	C^{4+} (wt%)	C^{4-} (wt%)	S^{6+} (wt%)	S^{2-} (wt%)	Layer thickness (m)	Density (g/cm^3)	Convergence rate (cm/yr)	Fe^{3+} (kg/yr/cm)	O_2Fe^{3+} equivalent (kg/yr/cm)	C^{4+} (kg/yr/cm)	C^{4-} (kg/yr/cm)	S^{6+} (kg/yr/cm)	S^{2-} (kg/yr/cm)	O_2C^{4+} equivalent (kg/yr/cm)	O_2S^{6+} equivalent (kg/yr/cm)
Input to Mariana convergent margin																		
Sediment	0.840	5.67	3.70	0.99	0.01	0.05	0.004	346	1.8	5.475	13	5.5	3.4	0.03	0.16	0.012	14	0.32
Altered oceanic crust	0.510	12.34	4.89	0.63	0	0.03	0.07	470	2.8		35	15	4.5	0	0.18	0.48	18	0.36
Dike unit	0.151	11.41	1.34	0.11	0	0	0.15	1530	2.8		31	13	2.6	0	0	3.5	10	0
Gabbro unit	0.107	11.67	0.97	0.08	0	0	0.11	5000	3.3		88	38	7.3	0	0	10	29	0
Serpentinized lithosphere	0.500	7.47	2.90	0.07	0	0.08	0.09	2400	2.8		107	46	2.6	0	2.9	3.2	10	5.7
										Total input	*274*	*118*	*20.4*	*0.03*	*3.2*	*17*	*81*	*6.4*
Pristine oceanic crust																		
Basalt	0.151	11.41	1.34	0.11	0	0	0.15	2000	2.8	5.475	41	18	3.4	0	0	4.6	14	0
Gabbro	0.107	11.75	0.97	0.08	0	0	0.15	5000	3.3		88	38	7.3	0	0	14	29	0
										Total pristine MORB	*129*	*55*	*10.7*	*0.0*	*0.0*	*19*	*43*	*0.0*
										Total surface oxidation in (Fe)	*145*	*62*	*9.7*	*0.03*	*3.2*	*0*	*38.7*	*6.4*
										Total surface oxidation in (Fe + C + S)		*107*						
										arc crust production rate (km^3/Myr/km)								
Output to Mariana convergent margin																		
Volcanic arc (min)	0.177	9.10	1.25	0.10		0.20			2.8	29	10	4.4	0.8	0	1.6	0	3.2	3.2
Volcanic arc (max)				0.20						50	18	7.5	2.8	0	2.8	0	11	5.6
Mantle contribution (min)	0.128	9.10	0.91	0.10			0.15				7.4	3.2	0.8	0	0	1.2	3.2	0
Mantle contribution (max)				0.10							13	5.5	1.4	0	0	2.1	5.6	0
Back-arc (min)	0.138	8.13	0.87	0.10			0.15	5500	2.8	1.5	20	8.6	2.3	0	0	3.5	9.2	0
Back-arc (max)				0.20						3.2	43	19	10	0	0	7.5	40	0
Mantle contribution (min)	0.128	8.13	0.81	0.10			0.15	5500	2.8		19	8.0	2.3	0	0	3.5	9.2	0
Mantle contribution (max)				0.10							40	17	5.0	0	0	7.5	20	0
										Total Marianas output (min)	*30*	*13*	*3.1*		*1.6*	*3.5*	*13*	*3.2*
										Total Marianas output (max)	*61*	*26*	*13*		*2.8*	*7.5*	*51*	*5.6*
										Total non-mantle oxidation out (min, Fe)	*4.1*	*1.8*	*0*		*1.6*	*0*	*0.0*	*3.2*
										Total non-mantle oxidation out (max, Fe)	*7.8*	*3.3*	*6.4*		*2.8*	*0*	*26*	*5.6*
										Total non-mantle oxidation out (min, Fe + C + S)	*5.8*	*5*						
										Total non-mantle oxidation out (max, Fe + C + S)	*17*	*34*						
										Surface oxidation input to the deep mantle		*68%–95%*						

[a] $Fe^{3+}/\Sigma Fe$ ratios for pristine oceanic crust, volcanic arc, and back-arc are constrained from Fe-XANES analyses of pristine glasses, following the methods of Cottrell et al. (2009) and Zhang et al. (2018). An alternative calibration for these measurements is available (Berry et al., 2018), which would decrease all $Fe^{3+}/\Sigma Fe$ ratios determined by Fe-XANES from the Cottrell/Zhang approach by ~0.04. The change does not impact the findings of this study. The reader is referred to Cottrell et al. (in press) for a discussion of the merits and flaws of each calibration.

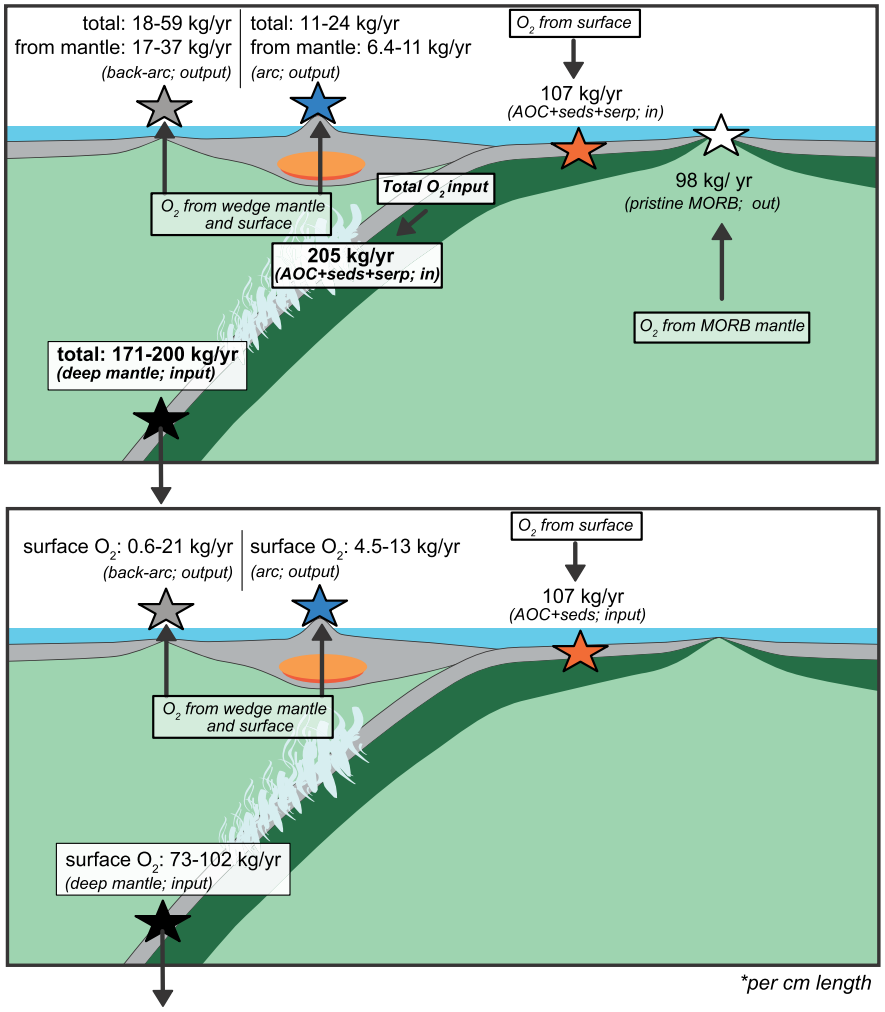

Fig. 3. (a) A diagram of the sum of O_2 (from Fe, S, and C) fluxes calculated here. The output of O_2 from the mantle as the result of the production of pristine MORB represents mantle-derived O_2. The input of O_2 to the mantle at subduction zones, in the form of altered oceanic crust, seafloor sediments, and serpentinized mantle lithosphere reflects O_2 from the mantle output at MORB plus additional, surface-derived O_2. The output of O_2 at arc and back-arcs reflect O_2 contributions from the mantle wedge, plus O_2 derived from the subducting slab (which itself contains O_2 from the surface and O_2 from the MORB mantle). The deep mantle O_2 input reflects the difference between the O_2 input at the subduction zone and the O_2 output at the arc and back-arc, and reflects contributions from surface-derived O_2 and MORB mantle-derived O_2. (b) the same as (a) but tracing only surface-derived oxygen, i.e., the O_2 acquired by the Pacific plate during sedimentation and alteration.

the 801 Super Composite powder, we take the same approach as for the sediments, and calculate a weighted average from reported measurements of individual lithologies (Floyd and Castillo, 1992; Table 3). For the dike and gabbro layers, we assume that these rocks are unaltered and contain no organic carbon or sulfate, and have carbonate and sulfide contents that sum to the concentrations dissolved in the same primary mid-ocean ridge mantle melt calculated above, from sample 801C-28R2-118 (Le Voyer et al., in press; Saal et al., 2002; Mathez, 1976; Table 4). We use values for each species from Evans (2012) for serpentinized mantle lithosphere. Substituting each species concentration for $[Fe^{3+}]_i$ in equation (1) above, we can calculate total input fluxes, and the equivalent O_2 necessary to balance C^{4+} as CO_3^{2-} and S^{6+} as SO_4^{2-}. The total input flux for sulfate is <4 S^{6+} and <7 equivalent O_2 kg/yr/cm arc length. The total input flux for sulfide is 17 kg/yr/cm arc length, organic carbon is 0.86 kg/yr/cm arc length, and carbonate is 20 kg/yr/cm arc length. The equivalent O_2 of the total input CO_3^{2-} flux is 81 kg/yr/cm arc length. As in the case for Fe, we calculate how much of this is due to alteration on the seafloor, and what may have been output originally at the mid-ocean ridge by considering what the "fresh", unaltered section at Site 801 looked like at the time of its creation on the ridge. We assume that unaltered oceanic crust contains no organic carbon or sulfate, and carbonate and sulfide concentrations equal to those dissolved in a primary mid-ocean ridge mantle melt, as above. While high-temperature ridge hydrothermal vent systems that are built on the ocean crust near spreading ridges precipitate significant quantities of sulfide and other reduced materials, site 801 materials show no evidence for this style of high-temperature hydrothermal mineralization. Thus, we do not consider them in the calculations presented here. Using the same procedure described above for iron, we estimate that pristine MORB has an output flux of 19 S^{2-} and 11 C^{4+} (and no S^{6+}, organic carbon; kg/yr/cm arc length). The difference in the fluxes for altered Pacific plate and pristine MORB (9.7 C^{4+}, 0.86 organic carbon, <4 S^{6+}, and 0 S^{2-} kg/yr/cm arc length) represents the total amount of each species produced as the result of alteration on the seafloor and the deposition of seafloor sediments on top of the oceanic crust between the time the crust was created and the time that the slab will be subducted (Table 2). For C^{4+}, this represents an uptake of 39 kg/yr/cm arc length equivalent O_2 during alteration on the seafloor, about 62% of the contribution from the presence of ferric iron. We explored the utility of adding Mn to this calculation, assuming that the total concentration of Mn in the sediment column is present as Mn^{4+} oxides that comprise manganese nodules, that Mn contained in the mantle and in MORB and arc primary magmas is present as Mn^{2+}, and that

altered oceanic crust contains the same amount of Mn^{2+} as primary magmas. If we add Mn^{4+} deposited into seafloor sediments from the ocean column, we find that additional ~0.7 kg/yr/cm arc length of surface-derived O_2 is input into the Mariana subduction system. This is small, and does not change the findings of this study.

4.3. Output of ferric iron and CO_2 at the Mariana arc and back-arc

To calculate the output flux of Fe^{3+} to the Mariana subduction system, we consider the magmatic output along the arc and back-arc. For the volcanic arc, we use an average primary melt $Fe^{3+}/\Sigma Fe$ ratio of 0.177 and FeO* of 9.1 wt%, calculated from Mariana arc basaltic melt inclusions and submarine glasses (Brounce et al., 2014). For the back-arc, we use an average primary melt $Fe^{3+}/\Sigma Fe$ ratio of 0.138 and FeO* of 8.13 wt%, calculated from Mariana trough submarine glass (Brounce et al., 2014; Kelley and Cottrell, 2009). The output flux can be calculated then using the equation,

$$F_{out} = \sum P_j * \rho_j * [Fe^{3+}]_j \quad (2)$$

where P_j is the production rate of crust in setting j (Dimalanta, 2002; Reymer and Schubert, 1984), ρ_j is the density of crust in setting j, and $[Fe^{3+}]_j$ is the Fe^{3+} concentration calculated for each setting. This yields a range of permissible output fluxes between 10 and 18 kg Fe^{3+}/yr/cm arc length for the volcanic arc and 20–43 kg Fe^{3+}/yr/cm arc length for the back-arc spreading center (calculated using equation (1), as described above for the input flux). The range in these values is controlled by the production rate of arc and back-arc crust, which varies by a factor of two in both settings, and exceeds uncertainty in any other values used here. To calculate the output flux of C^{4+}, S^{6+}, and S^{2-} to the Mariana subduction system, we use estimates of the undegassed carbon and sulfur contents of Mariana arc rocks of between 1000–3000 ppm C^{4+}, 2000 ppm S^{6+}, and no sulfide (Brounce et al., 2014; Wallace, 2005), and of Mariana back-arc spreading center rocks of between 1000–2000 ppm C^{4+}, 1500 ppm S^{2-}, and no sulfate (Brounce et al., 2014; Wallace, 2005), and substitute these values for $[Fe^{3+}]_j$ in equations (1) and (2), as described for Fe. The permissible output fluxes for each of these species is listed in Table 4.

In order to determine the subduction efficiency of oxidized materials, quantifying the contribution to the arc that comes solely from the subducted slab (and not from the mantle wedge) is key. To do this, we assume that the oceanic upper mantle is homogeneous with respect to fO_2 and equal to MORB source mantle. Primary melts of this mantle have an $Fe^{3+}/\Sigma Fe$ ratio = 0.117, independent of the extent of melting. We also assume that pressure of melting is the dominant control on the FeO* content of a primary mantle melt (Gale et al., 2013; Langmuir et al., 1992), so we assign arc and back-arc primary melts the same FeO* contents as those calculated above for arc (9.1 wt%) and back-arc (8.13 wt%) primary melts. We assign these melts undegassed C contents of 1000 ppm (Saal et al., 2002; Le Voyer et al., 2017), 1500 ppm S as sulfide (Wallace, 2005), and no sulfate. The mantle contribution is between 7.4–13 Fe^{3+}, 0.8–1.4 C^{4+}, and 1.2–2.1 S^{2-} (kg/yr/cm arc length) for the arc, and between 19–40 Fe^{3+}, 2.3–5.0 C^{4+}, and 3.5–7.5 S^{2-} (kg/yr/cm arc length) for the back-arc. Independent of the mantle contribution, the oxygen output flux from Fe^{3+}, C^{4+}, and S^{6+} for arc and back-arc magmatism combined is 5–34 O_2 (kg/yr/cm arc length). This represents the proportion of the oxidized signature of Mariana arc and back-arc magmas that cannot be accounted for by simple melting of the upper mantle, and thus may be sourced from the altered crust and sediments of the Pacific plate. When combined with our estimate of the oxygen acquired by the Pacific plate during sedimentation and alteration on the seafloor, we balance the flux of O_2 through the Mariana subduction system, yielding an excess of 73–102 O_2 kg/yr/cm arc length (68–95% of surface-derived O_2; Fig. 3) that is taken up during sedimentation and alteration of the Pacific plate and enters the subduction zone, but is not output from the arc or back-arc. Of this excess surface-derived oxygen that is subducted into the deep mantle, 18% is contained in seafloor sediments, 24% is contained in altered oceanic crust, and 58% is contained in serpentinized lithosphere. We also point out that even if serpentinized lithosphere is left out of the mass balance (e.g., because of the large uncertainties associated with the constraint), the sediments and altered oceanic crust portion of the Pacific plate contain enough surface-derived oxygen (46 kg/yr/cm) to produce the oxidized nature of arc basalts, and would leave an excess of 11–41 O_2 kg/yr/cm arc length (25–89% of surface-derived O_2) in the slab as it subducts into the deep mantle. Because the present configuration of the Mariana subduction system is an endmember configuration, i.e., the slab is among the oldest seafloor being subducted today and the thick sediment pile is entirely subducted, these calculations present the maximum abundance of surface derived O_2 into the mantle during subduction. We predict that the Cascadia margin, where a young slab subducts and some portion of sediments are scraped off the slab, carries a lower abundance of surface derived O_2 into the deep mantle.

4.4. Fate of oxidized materials

There are several possibilities for the fate(s) of the oxidized materials that are not output in the Marianas subduction system. First, the output flux calculation here does not include any output of oxidized fluids to the forearc, which is expressed in the Marianas through serpentine mud volcanism (Parkinson and Pearce, 1998) and fluid seeps (O'Hara et al., 2012). This output may be significant, particularly for carbon (e.g., Kelemen and Manning, 2015). Constraining the mass flux in this area is difficult because of the heterogeneity of materials coming out (fluids, mud, serpentinized xenolith blocks), the lack of redox information for most of these samples, and the large uncertainty in how pervasive this activity may be in the Mariana forearc. In particular, much of the Mariana seafloor lies below 6500 m water depth, which limits most manned and unmanned seafloor exploration, making the geophysical and geochemical condition of the deep ocean basins virtually unknown.

Second, it is possible that some or all of the excess Fe^{3+}, C^{4+}, S^{6+}, S^{2-}, or O_2 is transferred from subducting slabs to the mantle wedge and does not contribute to the oxidized nature of arc or back-arc magmas, for example, by serpentinizing mantle wedge peridotite. This is similarly difficult to assess because of the lack of a comprehensive understanding of the mechanisms and pathways for material transfer from subducting slab surfaces to volcanic arcs. For example, the fO_2 recorded by peridotites in the Tonga forearc is highly variable, and increases with increasing signatures of slab fluids (Birner et al., 2017), such that the portions of the mantle through which slab fluids percolate are oxidized, while other portions retain fO_2 indistinguishable from peridotites in a ridge setting.

A third possibility is that some or all of the excess Fe^{3+}, C^{4+}, S^{6+}, S^{2-}, and/or O_2 is retained in subducting slabs when it is subducted past the subduction systems and into the deep mantle. In this case, the excess oxidized signature would suffer the same fate(s) of deep subducted slabs, of which there are many possibilities. They may be subducted to the transition zone and/or the core mantle boundary, where they potentially contribute to the sources for mantle plumes. In this scenario, we would predict that EM-I, EM-II, or HIMU style plumes may have some portion of the return flux of the excess oxidized signatures from subduct-

ing slabs, because the isotopic signatures of these endmembers are hypothesized to be derived from subducted slabs, specifically seafloor sediments and/or altered oceanic crust (e.g., Zindler and Hart, 1986). If the alteration and oxidized nature of seafloor sediments and altered oceanic crust is the result of high pO_2 at Earth's surface, then only mantle plumes containing slabs that were at the surface after the Great Oxidation Event (~2.4 Ga; e.g., Lyons et al., 2014), or even later, after the timing of the oxygenation of the deep oceans (400–800 Ma; e.g., Lyons et al., 2014; Stolper and Keller, 2018) should produce oxidized ocean-island lavas today. Note that at this time, serpentinized slab lithosphere, the formation of which would not necessitate high pO_2 at Earth's surface, is not a leading hypothesis for the identity of EM-I, EM-II, or HIMU mantle components. If oxidized surface conditions were a prerequisite for generating oxidized OIB, we would expect only plumes that incorporate subducted slabs that are younger than 2.4 Ga, or perhaps only those that are younger than ~400–800 Ma, to contain the oxidized signatures of Earth's surface environments. Icelandic and Hawaiian primary magmas are oxidized and these observations have been attributed to presence of recycled slab materials that are younger than 2.4 Ga in each of the plumes (Brounce et al., 2017; Moussallam et al., 2016; Helz et al., 2017; Shorttle et al., 2015; McKenzie et al., 2004). Our results support these hypotheses in demonstrating quantitatively that altered oceanic crust and seafloor sediments contain significant amounts of oxidized materials after recycling takes place at subduction zones like the Marianas. We hypothesize that plumes with older recycled materials, such as perhaps Samoa and Reunion (e.g., Cabral et al., 2013; Andersen et al., 2015) will not be as oxidized.

5. Conclusions

We present the $Fe^{3+}/\Sigma Fe$ ratios of sediments and altered oceanic crust recovered from ODP Site 801 in Jurassic aged Pacific plate in order to constrain the bulk oxidation state of materials entering the Mariana subduction system. The overlying sediments are oxidized, ranging from 0.69 to >0.96 $Fe^{3+}/\Sigma Fe$, with three samples below the detection limit for Fe^{2+} in our analytical procedure. In the basaltic crust, minimally altered basalt ranges from 0.29 to 0.46 $Fe^{3+}/\Sigma Fe$, demonstrating that alteration leads to significantly increased $Fe^{3+}/\Sigma Fe$ ratios in igneous materials. Pervasively altered basalts are even more oxidized, with $Fe^{3+}/\Sigma Fe$ ratios from 0.47 to 0.78. The iron oxide veins, celadonite veins, and alteration halos included in these altered basalts range from 0.52 to 0.95 $Fe^{3+}/\Sigma Fe$ ratio. Composite powders meant to be representative of the bulk composition of the basement at ODP Site 801 are consistent with the $Fe^{3+}/\Sigma Fe$ ratios measured on discrete samples. In particular, the 801 Super Composite has $Fe^{3+}/\Sigma Fe$ equal to 0.51, broadly consistent with the oxidation state of Fe in various levels of altered basalts. These data are used to calculate a mass balance of Fe^{3+}, C^{4+}, S^{6+}, S^{2-}, and associated O_2 through the Mariana subduction system. We show that the fluxes of oxidized material into the Marianas are greater than the flux out of the subduction system along the volcanic arc and back-arc, and that 68–95% of the surface-derived oxygen taken up by the plate is not output back to the surface in the Mariana subduction system. Today, surface-derived oxygen from sediments (18% of total) and altered oceanic crust (24% of total) alone are in excess of arc output such that the Pacific plate carries excess oxygen to the deep Earth even when we consider the large uncertainties associated with serpentinized mantle lithosphere (58% of total). This indicates that altered oceanic plates stored in the mantle on long timescales may retain some oxidized components derived from alteration at Earth's surface, and if present in the mantle sources for some ocean-island volcanoes, may contribute to the production of oxidized, primary ocean island magmas. Our mass balance applies to altered oceanic crust that was altered at Earth's surface after the Great Oxidation Event (~2.4 Ga), or perhaps after the oxygenation of the deep oceans (400–800 Ma).

Acknowledgements

We would like to thank Terry Plank for generously contributing samples to this study. We are grateful for guidance from R. Lange and assistance from S. Grocke during wet chemical procedures. T. Rose kindly provided support in all laboratory endeavors. This submission was improved by constructive reviews from O. Rouxel, D. Canil, and an anonymous reviewer. We acknowledge support from Smithsonian's Scholarly Studies Program (EC), NSF MARGINS-EAR-0841108 (KK), NSF OCE-0961559 (KK), and NSF MARGINS-EAR-0841006 (EC).

Appendix A. Supplementary material

Supplementary material related to this article can be found online at https://doi.org/10.1016/j.epsl.2019.115859.

References

Andersen, M.B., Elliott, T., Freymuth, H., Sims, K.W., Niu, Y., Kelley, K.A., 2015. The terrestrial uranium isotope cycle. Nature 517, 356–359.
Andreani, M., Munoz, M., Marcaillou, C., Delacour, A., 2013. µXANES study of iron redox state in serpentine during oceanic serpentination. Lithos 178, 70–83.
Alt, J.C., Burdett, J.W., 1992. Sulfur in Pacific deep-sea sediments (Leg 129) and implications for cycling of sediment in subduction zone. Proc. Ocean Drill. Program Sci. Results 129, 283–294.
Alt, J.C., Muehlenbachs, K., Honnorez, J., 1986. An oxygen isotopic profile through the upper kilometer of the oceanic crust, DSDP hole 504B. Earth Planet. Sci. Lett. 80, 217–229.
Alt, J.C., Teagle, D.A.H., 2003. Hydrothermal alteration of upper oceanic crust formed at a fast-spreading ridge: mineral, chemical and isotopic evidence from ODP Site 801. Chem. Geol. 201, 191–211.
Berry, A.J., Stewart, G.A., O'Neill, H.St.C., Mallmann, G., Mosselmans, J.F.W., 2018. A re-assessment of the oxidation state of iron in MORB glasses. Earth Planet. Sci. Lett. 483, 114–123.
Birner, S.K., Warren, J.M., Cottrell, E., Davis, F.A., Kelley, K.A., Falloon, T.J., 2017. Forearc peridotites from Tonga record geterogeneous oxidation of the mantle following subduction initiation. J. Petrol. 58 (9), 1755–1780.
Brounce, M., Kelley, K.A., Cottrell, E., Reagan, M.K., 2015. Temporal evolution of oxygen fugacity during subduction initiation. Geology 43 (9), 775–778.
Brounce, M., Kelley, K.A., Cottrell, E., 2014. $Fe^{3+}/\Sigma Fe$ variations in Mariana arc basalts and primary fO_2 of the mantle wedge. J. Petrol. 55, 2513–2536.
Brounce, M., Stolper, E., Eiler, J., 2017. Redox variations in Mauna Kea lavas, the oxygen fugacity of the Hawaiian plume, and the role of volcanic gases in Earth's oxygenation. Proc. Natl. Acad. Sci. 114 (34), 8997–9002.
Cabral, R.A., Jackson, M.G., Rose-Koga, E.F., Koga, K.T., Whitehouse, M.J., Antonelli, M.A., Farquhar, J., Day, J.M.D., Hauri, E.H., 2013. Anomalous sulphur isotopes in plume lavas reveal deep mantle storage of Archaean crust. Nature 496, 490–493.
Cai, C., Wiens, D.A., Shen, W., Eimer, M., 2018. Water input into the Mariana subduction zone estimated from ocean-bottom seismic data. Nature 563, 389–392.
Carmichael, I.S.E., 2014. Chemical analysis of silicate rocks: a manual. IEDA, https://doi.org/10.1594/IEDA/100440.
Cottrell, E., Birner, S., Brounce, M.N., Davis, F., Waters, L., Kelley, K.A., (in press). Redox state as a geodynamic marker. AGU Monograph Series.
Cottrell, E., Kelley, K.A., 2011. The oxidation state of Fe in MORB glasses and the oxygen fugacity of the upper mantle. Earth Planet. Sci. Lett. 305 (3–4), 270–282.
Cottrell, E., Kelley, K.A., Lanzirotti, A., Fischer, R.A., 2009. High-precision determination of iron oxidation state in silicate glasses using XANES. Chem. Geol. 268, 167–179.
Dimalanta, C., 2002. New rates of western Pacific island arc magmatism from seismic and gravity data. Earth Planet. Sci. Lett. 202, 105–115.
D'Souza, R.J., Canil, D., 2018. The partitioning of chalcophile elements between sediment melts and fluids at 3 GPa, 950–1050 C with implications for slab fluids in subduction zones. Earth Planet. Sci. Lett. 498, 215–225.
Duncan, M.S., Dasgupta, R., Tsuno, K., 2017. Rise of Earth's atmospheric oxygen controlled by efficient subduction of organic carbon. Nat. Geosci. 10, 387–392.
Elliott, T., Plank, T., Zindler, A., White, W., Bourdon, B., 1997. Element transport from slab to volcanic front at the Mariana arc. J. Geophys. Res. 102 (B7), 14991–15019.
Evans, K.A., 2012. The redox budget of subduction zones. Earth-Sci. Rev. 113, 11–32.

Fisk, M., Kelley, K.A., 2002. Probing the Pacific's oldest MORB glass: mantle chemistry and melting conditions during the birth of the Pacific Plate. Earth Planet. Sci. Lett. 202 (3), 741–752.
Floyd, P.A., Castillo, P.R., 1992. Geochemistry and petrogenesis of Jurassic ocean crust basalts, Site 801. Proc. Ocean Drill. Program Sci. Results 129, 361–388.
Gaillard, F., Scaillet, B., Pichavant, M., Iacono-Marziano, G., 2015. The redox geodynamics linking basalts and their mantle sources through space and time. Chem. Geol. 418, 217–233.
Gale, A., Dalton, C.A., Langmuir, C.H., Su, Y., Schilling, J.-G., 2013. The mean composition of ocean ridge basalts. Geochem. Geophys. Geosyst. 14 (3), 489–518.
Gillis, K.M., Robinson, P.T., 1990. Patterns and processes of alteration in the lavas and dykes of the Troodos Ophiolite, Cyprus. J. Geophys. Res., Solid Earth 95 (B13), 21523–21548.
Hayes, J.M., Waldbauer, J.R., 2006. The carbon cycle and associated redox processes through time. Philos. Trans. R. Soc. 361, 931–950.
Helz, R.T., Cottrell, E., Brounce, M.N., Kelley, K.A., 2017. Olivine-melt relationships and syneruptive redox variations in the 1959 eruption of Kilauea volcano as revealed by XANES. J. Volcanol. Geotherm. Res. 33 (334), 1–14.
Karpoff, A.M., 1992. Cenozoic and Mesozoic sediments from the Pigafetta Basin, Leg 129, Site 800 and 801: mineralogical and geochemical trends of the deposits overlying the oldest oceanic crust. Proc. Ocean Drill. Program Sci. Results 129, 3–30.
Kato, T., et al., 1998. Initial results from WING, the continuous GPS network in the western Pacific area. Geophys. Res. Lett. 25, 369–372.
Kelemen, P.B., Manning, C.E., 2015. Reevaluating carbon fluxes in subduction zones, what goes down, mostly comes up. Proc. Natl. Acad. Sci., 201507889.
Kelley, K., Plank, T., Ludden, J., Staudigel, H., 2003. Composition of altered oceanic crust at ODP Sites 801 and 1149. Geochem. Geophys. Geosyst. 4 (6). https://doi.org/10.1029/2002gc000435.
Kelley, K., Plank, T., Farr, L., Ludden, J., Staudigel, H., 2005. Subduction cycling of U, Th, and Pb. Earth Planet. Sci. Lett. 234 (3–4), 369–383.
Kelley, K.A., Cottrell, E., 2009. Water and the oxidation state of subduction zone magmas. Science 325 (5940), 605–607.
Kelley, K.A., Cottrell, E., 2012. The influence of magmatic differentiation on the oxidation state of Fe in a basaltic arc magma. Earth Planet. Sci. Lett. 329–330, 109–121.
Klein, F., Bach, W., Jons, N., McCollom, T., Moskowitz, B., Berquo, T., 2009. Iron partitioning and hydrogen generation during serpentinization of abyssal peridotites from 15°N on the Mid-Atlantic Ridge. Geochim. Cosmochim. Acta 73, 6868–6893.
Lancelot, Y., Larsen, R.L., et al., 1990. Proc. Ocean Drill. Program, Initial Rep. 129. https://doi.org/10.2973/odp.proc.ir.129.1990. Ocean Drilling Program, College Station, TX.
Langmuir, C.H., Klein, E.M., Plank, T., 1992. Petrological systematics of mid-ocean ridge basalts: constraints on melt generation beneath ocean ridges. Geophys. Monogr. 71, 187–284.
Le Voyer, M., Hauri, E.H., Cottrell, E., Kelley, K.A., Salters, V.M., Langmuir, C.H., Hilton, D.R., Barry, P.H., Furi, E., in press. Carbon fluxes and primary CO_2 contents along the global mid-ocean ridge system. Geochem. Geophys. Geosyst.
Le Voyer, M., Kelley, K.A., Cottrell, E., Hauri, E.H., 2017. Heterogeneity in mantle carbon content from CO_2-undersaturated basalts. Nat. Commun. 8.
Lecuyer, C., Ricard, Y., 1999. Long-term fluxes and budget of ferric iron: implication for the redox states of the Earth's mantle and atmosphere. Earth Planet. Sci. Lett. 165, 197–211.
Lyons, T.W., Reinhard, C.T., Planavsky, N.J., 2014. The rise of oxygen in Earth's early ocean and atmosphere. Nature 506, 307–315.
Marcaillou, C., Munoz, M., Vidal, O., Parra, T., Harfouche, M., 2011. Mineralogical evidence for H_2 degassing during serpentinization at 300 °C/300 bar. Earth Planet. Sci. Lett. 303, 281–290.
Mathez, E.A., 1976. Sulfur solubility and magmatic sulfides in submarine basalt glass. J. Geophys. Res. 81, 4269–4276.
McKenzie, D., Stracke, A., Blichert-Toft, J., Albarede, F., Gronvold, K., O'Nions, R.K., 2004. Source enrichment processes responsible for isotopic anomalies in oceanic island basalts. Geochim. Cosmochim. Acta 68, 2699–2724.
Morris, J., Tera, F., 1989. ^{10}Be and ^{9}Be in mineral separates and whole rocks from volcanic arcs: implications for sediment subduction. Geochim. Cosmochim. Acta 53, 3197–3206.
Moussallam, Y., Edmonds, M., Scaillet, B., Peters, N., Gennaro, E., Sides, I., Oppenheimer, C., 2016. The impact of degassing on the oxidation state of basaltic magmas: a case study of Kilauea volcano. Earth Planet. Sci. Lett. 450, 317–325.
Moussallam, Y., Oppenheimer, C., Scaillet, B., Gaillard, F., Kyle, P., Peters, N., Hartley, M., Berlo, K., Donovan, A., 2014. Tracking the changing oxidation state of Erebus magmas, from mantle to surface, driven by magma ascent and degassing. Earth Planet. Sci. Lett. 393, 200–209.
Mungall, J., 2002. Roasting the mantle: slab melting and the genesis of major Au and Au-rich Cu deposits. Geology 30 (10), 915–918.
O'Hara, Y., Reagan, M., Fukjikura, K., Watanabe, H., Martinez, F., Girard, G., Ribiero, J., Brounce, M., Komori, N., Kino, M., 2012. A serpentine-hosted ecosystem in the Southern Mariana Forearc. Proc. Natl. Acad. Sci. 109, 2177–2180.
Parkinson, I.J., Arculus, R.J., 1999. The redox state of subduction zones: insights from arc-peridotites. Chem. Geol. 160 (4), 409–424.
Parkinson, I.J., Pearce, J.A., 1998. Peridotites from the Izu-Bonin-Mariana forearc (ODP Leg 125): evidence for mantle melting and melt-mantle interaction in a supra-subduction zone setting. J. Petrol. 39 (9), 1577–1618.
Plank, T., et al., 2000. Proc. Ocean Drill. Program, Initial Rep. 185. https://doi.org/10.2973/odp.proc.ir.185.2000. Ocean Drilling Program, College Station, TX.
Plank, T., Langmuir, C.H., 1998. The chemical composition of subducting sediment and its consequences for the crust and mantle. Chem. Geol. 145, 325–394.
Reymer, A., Schubert, G., 1984. Phanerozoic addition rates to the continental crust and crustal growth. Tectonics 3, 63–77.
Rouxel, O., Dobbek, N., Ludden, J., Fouquet, Y., 2003. Iron isotope fractionation during oceanic crust alteration. Chem. Geol. 202 (1–2), 155–182.
Rouxel, O., Ono, S., Alt, J., Rumble, D., Ludden, J., 2008. Sulfur isotope evidence for microbial sulfate reduction in altered oceanic basalts at ODP Site 801. Earth Planet. Sci. Lett. 268, 110–123.
Ryan, W.B.F., et al., 2009. Global multi-resolution topography synthesis. Geochem. Geophys. Geosyst. 10 (3). https://doi.org/10.1029/2008gc002332.
Saal, A.E., Hauri, E.H., Langmuir, C.H., Perfit, M.R., 2002. Vapour undersaturation in primitive mid-ocean-ridge basalt and the volatile content of Earth's upper mantle. Nature 419, 451–455.
Sadofsky, S.J., Bebout, G.E., 2004. Nitrogen geochemistry of subducting sediments: new results from the Izu-Bonin-Mariana margin and insights regarding global nitrogen subduction. Geochem. Geophys. Geosyst. 5 (3). https://doi.org/10.1029/2003GC000543.
Shorttle, O., Moussallam, Y., Hartley, M.E., Maclennan, J., Edmonds, M., Murton, B.J., 2015. Fe-XANES analyses of Reykjanes Ridge basalts: implications for oceanic crust's role in the solid Earth oxygen cycle. Earth Planet. Sci. Lett. 427, 272–285.
Sleep, N.H., Bird, D.K., Pope, E., 2012. Paleontology of Earth's mantle. Annu. Rev. Earth Planet. Sci. 40 (1), 277–300.
Stolper, D.A., Keller, C.B., 2018. A record of deep-ocean dissolved O_2 from the oxidation state of iron in submarine basalts. Nature 553, 323–327.
Wallace, P.J., 2005. Volatiles in subduction zone magmas: concentrations and fluxes based on melt inclusion and volcanic gas data. J. Volcanol. Geotherm. Res. 140, 217–240.
Wilson, A.D., 1960. The micro-determination of ferrous iron in silicate minerals by a volumetric and a colorimetric method. Analyst 85 (1016), 823–827.
Wood, B.J., Bryndzia, L.T., Johnson, K.E., 1990. Mantle oxidation state and its relationship to tectonic environment and fluid speciation. Science 248 (4953), 337–345.
Zhang, H., Cottrell, E., Solheid, P., Kelley, K.A., Hirschmann, M.M., 2018. Determination of $Fe^{3+}/\Sigma Fe$ of XANES basaltic glass standards by Mossbauer spectroscopy and its application to the oxidation state of iron in MORB. Chem. Geol. 479, 166–175.
Zindler, A., Hart, S., 1986. Chemical geodynamics. Annu. Rev. Earth Planet. Sci. 14, 493–571.